crystals

Article

A Deep-Ultraviolet Photodetector of a Hybrid Organic-Inorganic p-CoPc/n-Ga_2O_3 Heterostructure Highlighting Ultra-Sensitive

Xiaohui Qi [1], Xueqiang Ji [1], Jianying Yue [1], Song Qi [1], Jinjin Wang [1], Peigang Li [1,*] and Weihua Tang [1,2,*]

[1] State Key Laboratory of Information Photonics and Optical Communications, School of Science, Beijing University of Posts and Telecommunications, Beijing 100876, China
[2] College of Integrated Circuit Science and Engineering, Nanjing University of Posts and Telecommunications, Nanjing 210023, China
* Correspondence: pgli@bupt.edu.cn (P.L.); whtang@njupt.edu.cn (W.T.)

Abstract: A practical method for organic–inorganic hybrid heterojunction photodetector by spin-coating the cobalt phthalocyanine (CoPc) solution onto the β-gallium oxide (β-Ga_2O_3) film is available to realize the sensitive detection of ultraviolet light signals. We have carefully measured and calculated the optoelectronic performance of the prepared device. The device demonstrates excellent rectification characteristics under different light intensities, and the rectification ratio reaches 144.96 under 900 $\mu W/cm^2$ at ±5 V. Benefiting from the construction of CoPc/Ga_2O_3 heterojunction, the device shows an extremely low dark current of 5.73 fA, a high detectivity of 1.92×10^{17} Jones, a responsivity of 18.4 mA/W, and a high light-to-dark current ratio of 3.76×10^6. In addition, the intrinsic physical mechanism of the device is investigated through the energy band diagram under different conditions. The device is equipped with the possibility to work under self-powered mode and has good stability in the air environment.

Keywords: deep-ultraviolet detection; heterojunction; Ga_2O_3

check for updates

Citation: Qi, X.; Ji, X.; Yue, J.; Qi, S.; Wang, J.; Li, P.; Tang, W. A Deep-Ultraviolet Photodetector of a Hybrid Organic-Inorganic p-CoPc/n-Ga_2O_3 Heterostructure Highlighting Ultra-Sensitive. *Crystals* **2022**, *12*, 1284. https://doi.org/10.3390/cryst12091284

Academic Editors: Pier Carlo Ricci and Dmitri Donetski

Received: 4 July 2022
Accepted: 8 September 2022
Published: 11 September 2022

1. Introduction

Ultra-wide bandgap semiconductor materials, generally with bandgaps of approximately 3.0 to 6.0 eV, are opening up a fascinating and challenging new area in the field of semiconductor materials, quantum information, and functional applications. Beccause some characteristics of wide bandgap semiconductor devices are non-linearly related to the bandgap, they are of higher research value than conventional semiconductor devices [1]. From the view of device structure, low-dimensional devices have fewer defects and higher crystal quality compared with bulk structure devices, thus offering better performance [2]. The ultra-sensitive and ultra-fast nature of two-dimensional (2D) materials in optoelectronic systems led it quickly extending to ultraviolet detection [3]. Most of the ultraviolet radiation from the Sun are absorbed by the stratospheric ozone layer, so the 200 to 280 nm is known as the solar-blind region. Ultraviolet detection has profound impacts on the military and civilian areas, including missile flame sensing, climate monitoring, chemical analysis, and space communication [4]. Therefore, the fabrication of ultraviolet photodetectors based on 2D wide bandgap semiconductor materials is imperative.

In recent years, a series of wide bandgap semiconductors have been applied to ultraviolet photodetectors, such as GaN, SiC, ZnO, Ga_2O_3, ZnMgO, etc. [5]. As a kind of direct bandgap semiconductor, Ga_2O_3 is emerging as the most promising candidate because of its excellent properties [6]. Ga_2O_3 has higher electron mobility, higher breakdown field strength, and higher Baliga's figure of merit (more than 3000) [7]. Ga_2O_3 has an ideal bandgap of about 4.7 to 4.9 eV, which is well-matched with the solar-blind region, and thus it can better realize ultraviolet detection [8]. Among the five different polymorphs (α, β, γ, δ, and ε) of Ga_2O_3, the β-phase has the best physical and chemical stability and is therefore the most widely studied phase. β-Ga_2O_3 has a monoclinic structure with space group C2/m and it has a melting point of up to 1720 °C [9,10]. In many specific design types of the device, photovoltaic devices are more popular than others due to their superior responsivity and the mature preparation process. Because Ga_2O_3 is an intrinsic n-type semiconductor, the heterojunction photodetector based on Ga_2O_3 is considered to be a practical solution [11]. Bae et al. reported a Cu_2O/Ga_2O_3 p-n heterostructure ultraviolet photodetector prepared by mechanical transfer methods [12]. Ding et al. fabricated an ultraviolet sensor based on GaN/Ga_2O_3 nanowire heterojunctions by chemical vapor deposition, which has good spectral selectivity [13]. Li et al. present a hybrid inorganic-organic Ga_2O_3/PEDOT:PSS 2D heterojunction ultraviolet photodetector with a fast response speed [14].

Organic thin film semiconductors are gaining importance due to their tremendous potential for organic electronics and optoelectronic devices. The performance of organic photovoltaic devices is highly dependent on the quality of the organic film semiconductor, highly uniform and continuous films would contribute to the transport of electrons [15]. The introduction of organic semiconductor layers in heterojunctions can improve unmatched deposition compatibility and device performance [16]. Metal phthalocyanines (MPc) are macrocyclic organic semiconductors with an 18π electron conjugated arrangement, and were first discovered to be semi-conductive in 1948 [17]. The derivatives of phthalocyanines are usually non-toxic, and also have good photoconductivity, physical stability, and chemical stability [18]. The cobalt phthalocyanine (CoPc), as one of the metal phthalocyanines, exhibits a p-type conductivity and high hole mobility [19]. CoPc has been studied widely in theory and practice for its many intriguing characteristics. The thermal stability of CoPc enables it can be used in temperature sensors, and the hydrophobicity of CoPc makes it very suitable for humidity sensors [20]. Meanwhile, CoPc has been used in heterojunctions for ultraviolet detection. Xiao et al. fabricated a self-powered ultraviolet sensor based on n-type porous-GaN/p-type CoPc heterojunctions with high switching ratios [21]. However, a CoPc/Ga_2O_3 heterojunction ultraviolet photodetector has not been reported so far.

In this work, we fabricated a planar heterojunction device based on an n-type Ga_2O_3 film and a p-type CoPc film with a combination of spin-coating and MOCVD methods. The device is highly sensitive to deep ultraviolet light, benefiting from the absorption selectivity of Ga_2O_3 and the construction of heterojunction. The built-in electric field at the heterojunction interface offers the potential for the self-powered operation of the device. X-ray diffraction (XRD) and ultraviolet-visible (UV-vis) were used to examine the quality of Ga_2O_3 and CoPc films. The *I-V* and *I-t* curves of the heterojunction devices were tested at various optical powers and voltages. The experiments indicate that the device has excellent rectification characteristics and stable periodic light response. In addition, the device has a high photo-to-dark current ratio and low dark current.

2. Experimental

2.1. Syntheses of CoPc Precursor Solution

Cobalt phthalocyanine (CoPc, purity $\geq$ 92%) and N,N-Dimethylformamide (DMF, 99%) was purchased from Anhui Cool Biological Engineering Co., Ltd. (Hefei, China) and Shanghai Macklin Biochemical Co., Ltd. (Shanghai, China). Ten mg of CoPC and one mL of DMF were added into the glass tube and the clear purple precursor solution was obtained after magnetic stirring for 30 min, as shown in Figure 1a. Figure 1b shows the molecular structures of CoPc.

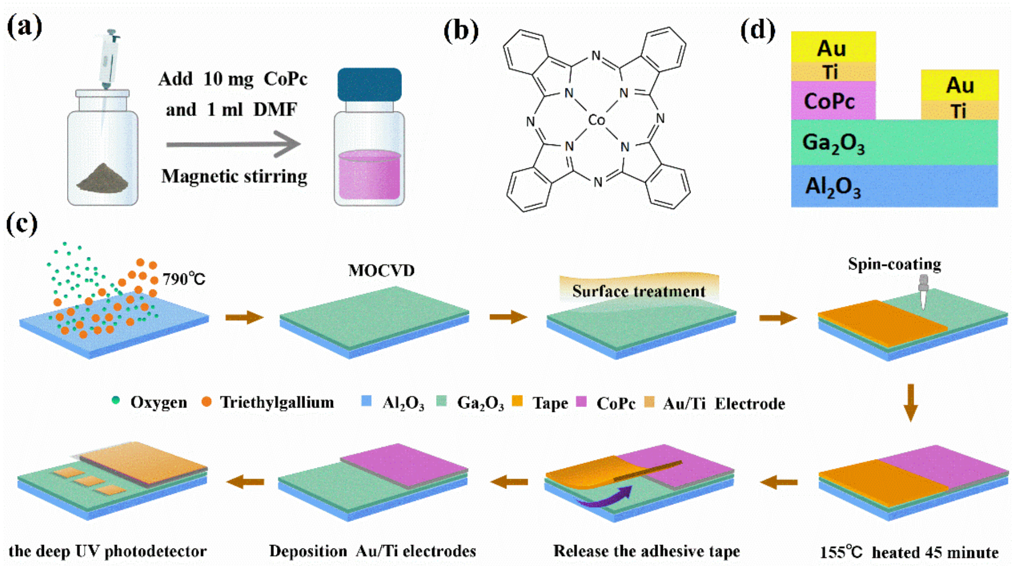

Figure 1. (**a**) Procedures for preparing the CoPc precursor solution. (**b**) Molecular structure of the semiconductor CoPc. (**c**) The fabrication of the CoPc/Ga_2O_3 heterojunction ultraviolet photodetector. (**d**) The cross-section of fabricated devices.

2.2. Syntheses of β-Ga_2O_3

Al_2O_3 substrates were purchased from Hefei Kejing Materials Technology Co., Ltd. (Hefei, China). The Ga_2O_3 film was deposited on Al_2O_3 (0001) substrates by metal-organic chemical vapor deposition (MOCVD). The oxygen (O_2), the triethylgallium (TeGa), and the argon (Ar) were selected as the O source, the Ga source, and the carrier gas, respectively. The flow rate of argon was 65 sccm. The reaction chamber temperature was 790 °C.

2.3. Fabrication of β-Ga2O3/CoPc Heterojunction Device

The preparation process of the heterojunction device is depicted in Figure 1c. The Ga_2O_3 film was ultrasonically cleaned with acetone, alcohol, and deionized water successively to remove contaminants and improve wettability. The Ga_2O_3 film was cut into small pieces (10 mm^2) by laser, and half of the small piece was covered with tape. Twenty μL of CoPc precursor solution was taken with a pipette and dropped onto the Ga_2O_3 surface. The spin-coating speed was first 600 rpm for 5 s and then 1500 rpm for 25 s. The two different speeds would result in a more uniform surface. After annealing at 155 °C for 45 min on a heating table, the tape was removed. Au/Ti electrodes were deposited on the surface of Ga_2O_3 and CoPc films by direct-current magnetron sputtering. The area between electrodes is 0.02 mm^2. The schematic diagram of the cross section of the device is shown in Figure 1d.

2.4. Characterization

The crystal quality was examined by XRD (X'Pert PRO, PANalytical) with a Cu K_α (λ~1.5405 Å) radiation, the scanning step is 0.02°. The absorption spectrum was measured by UV-vis (UV-1900, Macy), which can measure in the range of 190–1100 nm. The 254 nm beam was from the mercury lamp (Philips, Amsterdam, The Netherlands, TUV 8W), and the light intensity is changed by adjusting the lamp position. The dark condition was achieved by a closed black metal experiment box. Semiconductor analyzer (Keithley 4200) was employed to measure *I-V* and *I-t* curves under dark and light conditions.

3. Results and Discussion

The crystalline structure of the Ga_2O_3 and Al_2O_3 phases is characterized by XRD patterns. In Figure 2a, the diffraction peaks located at 18°, 38°, and 59° are attributed to the ($\bar{2}$01), ($\bar{4}$02), and ($\bar{6}$03) crystal planes of β-Ga_2O_3(JCPDS #43-1012). The results show that the prepared Ga_2O_3 is in β-phase. The sharpest peak at 18° indicates that the growth direction of the β-Ga_2O_3 phase is along the ($\bar{2}01$) direction. All the peak locations and corresponding intensities are well matched to the β-Ga_2O_3 [10]. In Figure 2b, the linear *I-V* curves of Au/Ti-Ga_2O_3 and Au/Ti-CoPc under dark conditions demonstrate that good Ohmic contacts would not affect the output performance of the heterojunction. In Figure 2c,d, the optical absorption spectrum of the prepared Ga_2O_3 film and CoPc film were measured on sapphire substrates to investigate their optical features. The prepared Ga_2O_3 has a sharp absorption edge around 255 nm, and the bandgap is estimated to be 4.85 eV. The absorption curve of the CoPc film has two main bands, one in the ultraviolet region, called Q-band, the other in the visible region, called B-band, which has a shoulder peak at about 700 nm. According to the absorption curve, we calculated the bandgap values of 1.55 eV and 1.80 eV for the B-band and 3.34 eV for the Q-band. All the results of the optical absorption tests and bandgap calculations are in high agreement with the previous work reported [22–24]. Figure 2e show the semi-log scale *I-V* curves of Ga_2O_3 single device under dark and 300 μW/cm^2 illumination. Figure 2f show the semi-log scale *I-V* curves of CoPc/Ga_2O_3 heterojunction device under the same conditions. In comparison with the single device, it is easy to see that the light response of the heterojunction device is obviously improved and has a significant rectification characteristic, which is attributed to the construction of the heterojunction and the formation of built-in electric field [25]. It is worth mentioning that the heterojunction device has an extremely low dark current, measured to be 5.73 fA, 1.57 fA, and 2.59 fA at 5 V, 0 V, and −5 V, respectively.

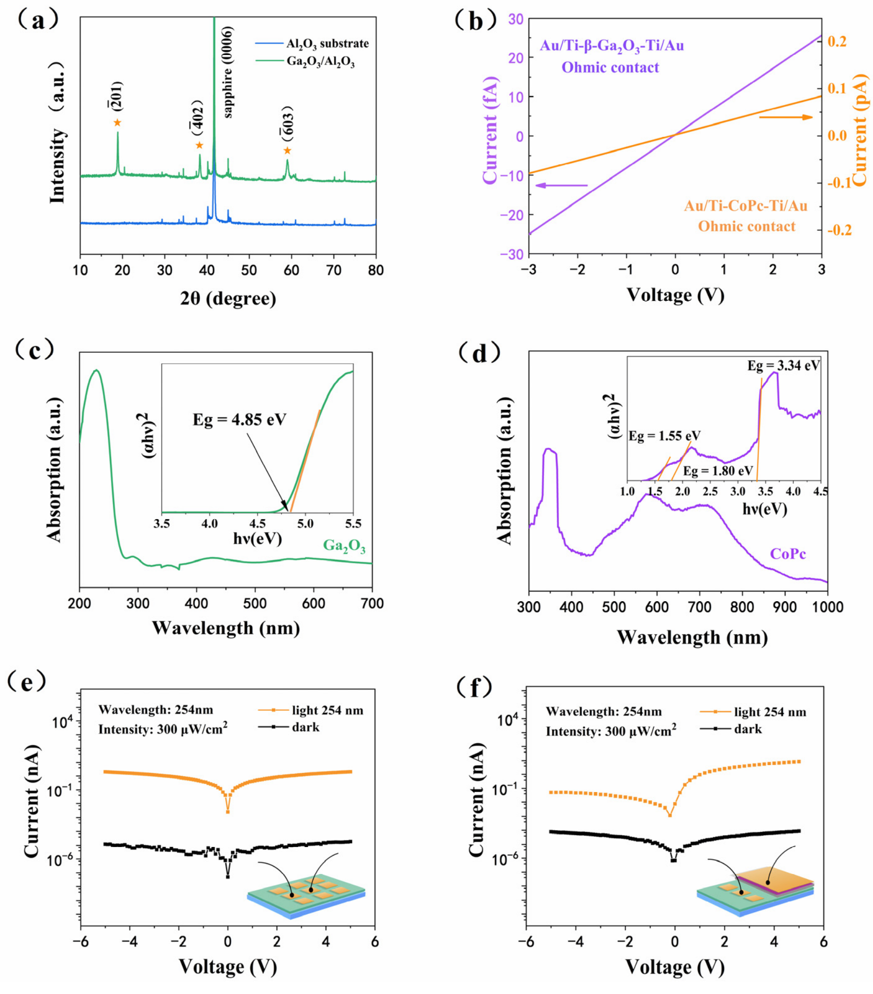

Figure 2. (**a**) The XRD patterns of Ga_2O_3/Al_2O_3 films by MOCVD. (**b**) The *I-V* curves of Au/Ti-Ga_2O_3-Ti/Au and Au/Ti-CoPc-Ti/Au under dark. The optical absorption curves of (**c**) Ga_2O_3 film and (**d**) CoPc film; inserts represent the estimated bandgaps. The semi-log scale *I-V* curves of (**e**) Ga_2O_3 film and (**f**) CoPc/Ga_2O_3 heterostructure.

We have carefully measured the *I-V* curves of the heterojunction device at various light intensities. The *I-V* curves for the light intensity ranges of 0.1–0.9 μW/cm^2, 1–9 μW/cm^2, 10–90 μW/cm^2 and 100–900 μW/cm^2 are displayed in Figure 3a–d, respectively. The test results indicate that the device is very sensitive to changes in ultraviolet light intensity and has a wide sensing test range. The device is capable of detecting weak UV signals even at 0.1 μW/cm^2, and still has good discrimination for light intensities less than 1 μW/cm^2. With increasing light intensity, the photocurrent of the heterojunction gradually increases because of the absorption of more photons in the photosensitive region and thus the excitation of more photogenerated carriers [26]. No matter how the light intensity changes, the device shows outstanding rectification characteristics. Under the light intensity of 900 μW/cm^2, the rectification ratio of the device reaches 144.96 at ±5 V. The photocurrents in different light intensity ranges at 5 V are shown in Figure 3e,f, respectively. The relationship between photocurrent and light power can be fitted by the following formula: $I_{ph} \propto P^{\theta}$, where I_{ph}, P, and θ are photocurrent, light power, and empirical coefficient. For different light intensity ranges, the values of θ were fitted to 0.97, 0.93, 0.91, and 0.88, respectively. The linearity of the photocurrent decreases with increasing light intensity because large light intensity increases the scattering of carriers and the chance of recombination of electron-hole pairs. The unavoidable defect states in the semiconductor film preparation process would also become the recombination centers of carriers [14].

The stability of the device's response to light has become the touchstone for measuring device performance. In Figure 4a, the *I-t* curves were measured with periodical on/off ultraviolet illumination with a light intensity of 100 to 900 μW/cm^2 at 5 V. The photocurrent increases steadily as the light intensity increases, the device can instantaneously respond to ultraviolet light and has a stable photoresponse at different light intensities. The *I-t* curves were measured with periodic on/off ultraviolet illumination with voltages from 1 to 5 V under 1000 μW/cm^2 light intensity, as shown in Figure 4b. As the voltage increases the photocurrent increases, the high voltage not only reinforces the diffusion rate of photogenerated carriers but also inhibits the recombination of electron-hole pairs [27]. A constant photocurrent can be obtained by controlling the external voltage of the device. In Figure 4c, the *I-t* curves were measured with periodical on/off ultraviolet illumination of light intensities from 10 to 90 μW/cm^2 at 0 V. The device can generate photocurrent without external voltage, and the photocurrent will change with light intensity, demonstrating that the device has the possibility to work well under self-powered mode. The typical overshoot feature of photocurrent comes from the increased carrier concentration in a short period of time. Substantial amounts of electrons and holes would not be extracted from the heterojunction timely because the voltage of the built-in electric field is too small [28]. This phenomenon can be alleviated by the applied voltage in Figure 4a,b. In general, the device is sensitive to ultraviolet light and has a stable periodic response at different voltages and different light intensities. For a more detailed comparison of the *I-t* curves, we further analyzed the response speed of the devices. An enlarged graph of one cycle period with 90 μW/cm^2 under self-powered mode was shown in Figure 4d. The rise and decay time (τ_r and τ_d) are tested for times when the photocurrent rises from 10 to 90% and falls from 90 to 10%, which are estimated to be 5.09 s and 7.51 s, respectively. The response time in self-powered mode is slow because the driving force of the built-in electric field is not enough to make the carriers flow at a faster rate. Figure 4e show the fitted *I-t* curves for Ga_2O_3 single device with 300 μW/cm^2 at 3 V. Figure 4f show the fitted *I-t* curves for CoPc/Ga_2O_3 heterojunction device under the same conditions. The rise and decay time are fitted according to the second-order exponential equation: $I = I_0 + Ae^{-t/\tau_1} + Be^{-t/\tau_2}$, where I_0 is the steady-state photocurrent, A and B are constants, τ_1 and τ_2 are relaxation constants. The rise and decay time (τ_{r1} and τ_{d1}) of the CoPc/Ga_2O_3 heterojunction are fitted to be 0.18 s and 0.35 s, which are faster than the former, demonstrating the construction of heterojunction could enhance the response speed of the device [29].

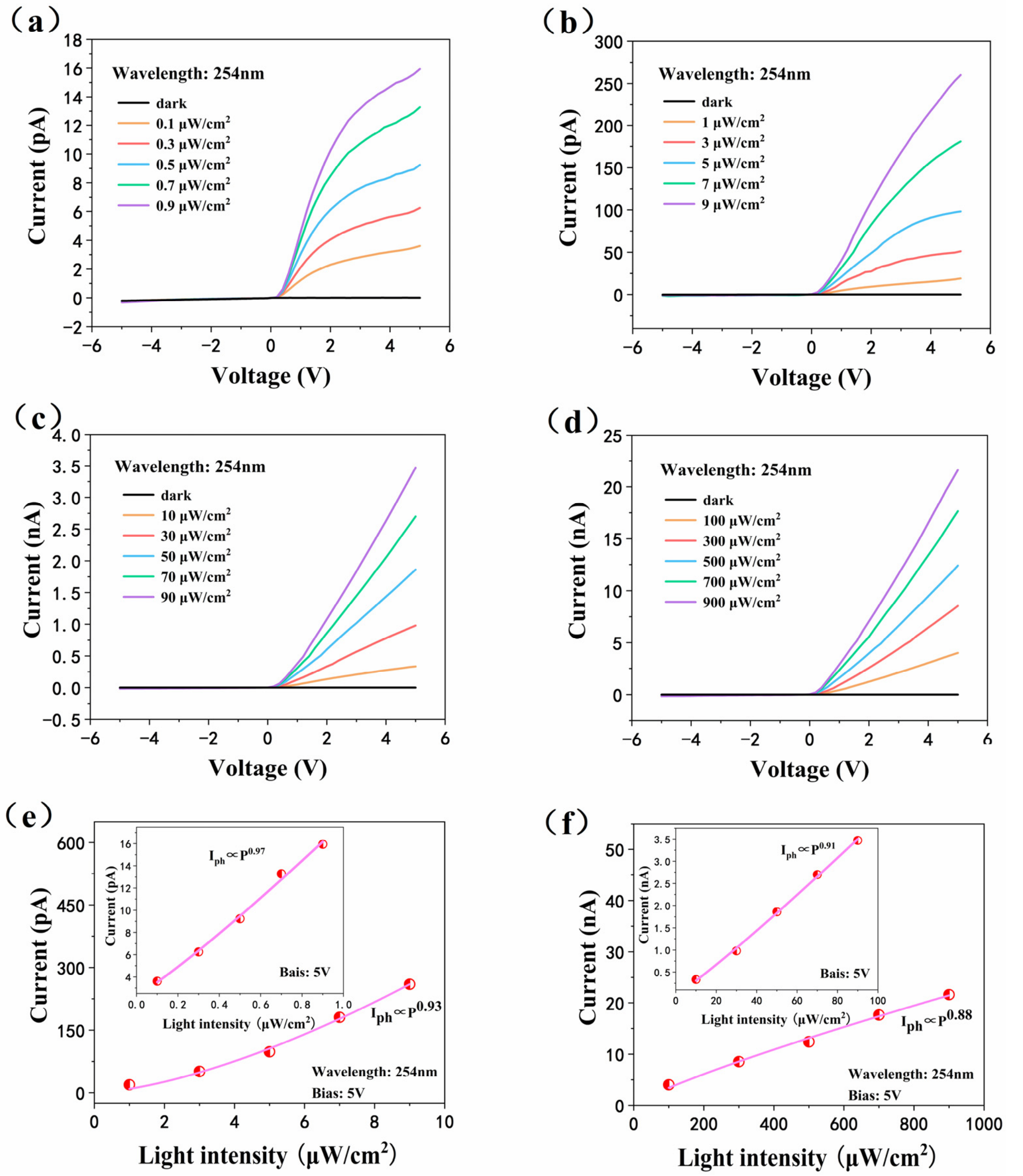

Figure 3. The *I-V* curves of the heterojunction device with various light powers: (**a**) 0.1–0.9 μW/cm^2, (**b**) 1–9 μW/cm^2, (**c**) 10–90 μW/cm^2, and (**d**)100–900 μW/cm^2. The photocurrents of heterojunction device with various light powers under 5 V: (**e**) 1–9 μW/cm^2 (insert was 0.1–0.9 μW/cm^2) and (**f**) 100–900 μW/cm^2 (insert was 10–90 μW/cm^2).

In order to further evaluate the photoelectric characteristics of the CoPc/Ga_2O_3 heterojunction device, some parameters of importance are analyzed here, including responsivity (*R*), detectivity (*D**), and photo-to-dark current ratio (*PDCR*). The responsivity is defined as the photocurrent produced per unit incident photon, representing the response efficiency of the device to the optical signal. The detectivity is defined as the noise figure of the device, reflecting the device's ability to detect weak optical signals in the noise environment. *PDCR* is defined as the signal-to-noise ratio of the device, representing the ability to resist noise. *R*, *D**, and *PDCR* can be expressed by the following formulas: $R = \left(I_{ph} - I_d\right)/P_\lambda S$, $D^* = R/(2eI_d/S)^{1/2}$ and $PDCR = \left(I_{ph} - I_d\right)/I_d$, where I_{ph}, I_d, P_λ, S, and e are photocurrent, dark current, incident light power, effective area, and electron charge, respectively. Figure 5a shows the variation of *R* and *D** with the applied voltage at 0.1 μW/cm^2 light intensity. The results show that *R* and *D** have the same trend, which both increase as the forward or negative voltage increases. When the voltage is 5 V, the

R-value is 18.4 mA/W, and the *D**-value is as high as 1.92×10^{17} Jones, which shows the excellent detection ability of the device. Figure 5b shows the variation of *PDCR* with light intensity at different voltages. The results show that *PDCR* increases with increasing light intensity at the same voltage. With the light intensity of 900 µW/cm^2, the *PDCR*-values are 5.04×10^5 and 3.76×10^6 at 1 V and 5 V, which reveal the good noise immunity of the device.

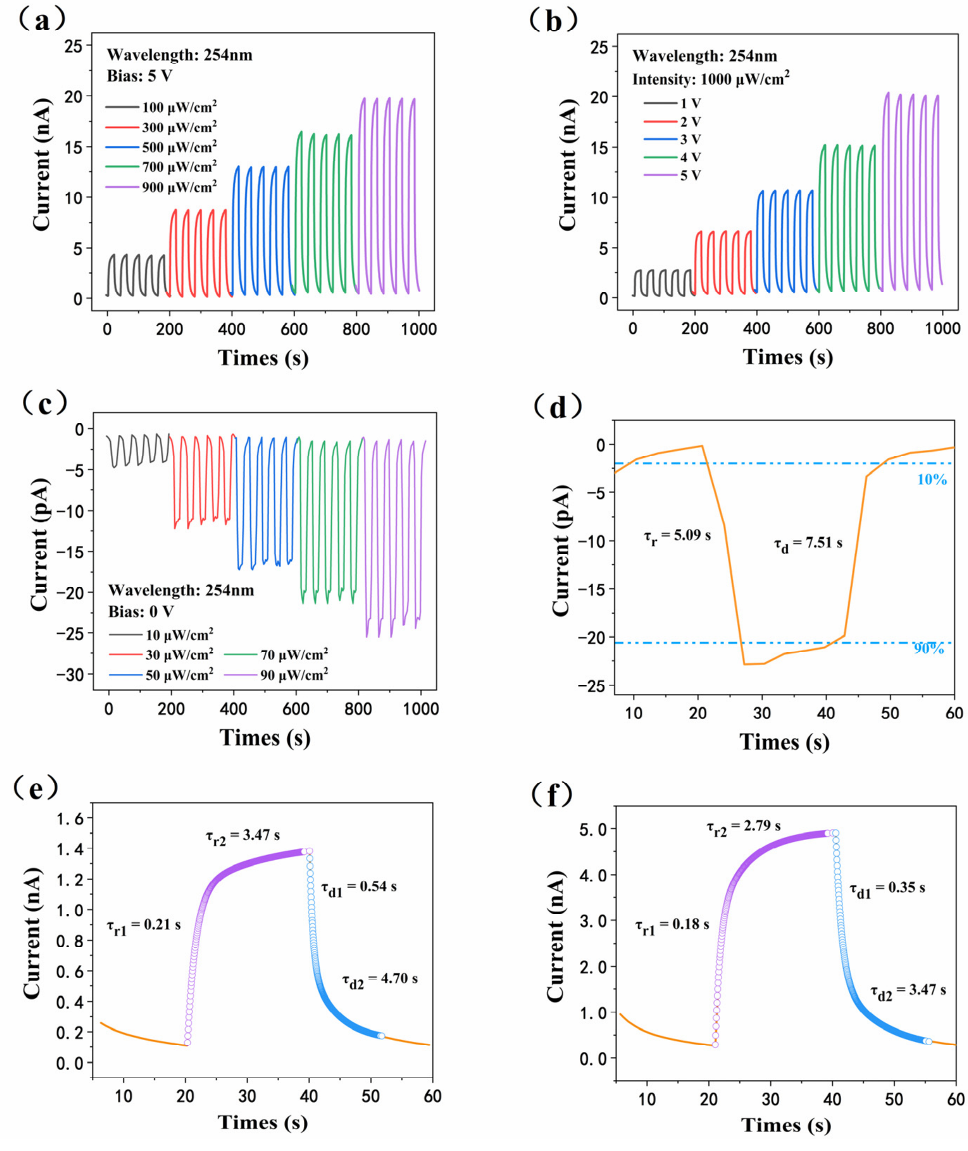

Figure 4. *I-t* curves of the heterojunction device. (**a**) Various light powers under 5 V, (**b**) various voltages under 1000 µW/cm^2, and (**c**) various light powers under 0 V. (**d**) The rise and decay time of the heterojunction device with 90 µW/cm^2 under 0 V. The rise and decay time of (**e**) Ga_2O_3 film and (**f**) CoPc/Ga_2O_3 heterojunction with 300 µW/cm^2 under 3 V.

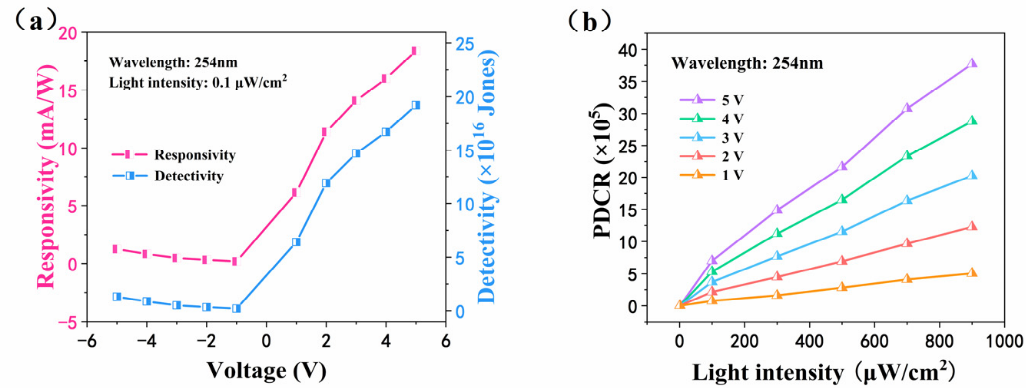

Figure 5. (**a**) The responsivity (*R*) and the detectivity (D^*) of the heterojunction device with an intensity of 0.1 mW/cm^2 under different voltages from −5 V to 5 V, voltage step is 1 V. (**b**) The *PDCR* versus different light intensities under 1 V, 2 V, 3 V, 4 V, and 5 V, respectively.

For an integrated understanding of the operating mechanism of the CoPc/Ga_2O_3 heterojunction device, the energy band alignment before contact and after contact are shown in Figure 6a,b, under dark and 254 nm light are shown in Figure 6c,d, and under forward and reverse voltage are shown in Figure 6e,f. Combining the bandgap calculation results in this work with previous reports, the conduction band (*Ec*) and valence band (*Ev*) of Ga_2O_3 were determined to be 4.0 eV and 8.85 eV, the lowest unoccupied molecular orbital (*LUMO*) and highest occupied molecular orbital (*HOMO*) of CoPc were determined to be 3.4 eV and 4.95 eV [16,30]. The work functions of Ga_2O_3 and CoPc are 4.06 eV and 4.4 eV, respectively [30,31]. The band bending is caused by the difference in the Fermi energy levels of Ga_2O_3 and CoPc. According to Anderson's law, the offsets of the conduction band and valence band (ΔEc and ΔEv) were determined to be 0.6 eV and 3.9 eV, respectively [32]. The noise of the heterojunction comes mainly from the dark current. The lower dark current of the device is due to rare intrinsic carriers without illumination. After the contact between Ga_2O_3 and CoPc, electrons flow from Ga_2O_3 to CoPc, and holes flow from CoPc to Ga_2O_3. In order to maintain the equilibrium of the Fermi energy levels of the heterostructure, the energy band of Ga_2O_3 would move lower and bend upward at the interface, and the energy band of CoPc would move higher and bend downward at the interface. With the diffusion movement of carriers, the built-in electric field is formed at the heterojunction interface, and the formation of the space charge region leads to the depletion layer [33]. When the device exposed to ultraviolet light, the electron-hole pairs are excited in Ga_2O_3, which are separated under the effect of the built-in electric field and flow to the corresponding electrodes, resulting in a circuit inside the heterojunction, so the device can operate under self-powered mode. When a forward voltage is applied to the device, the direction of the external voltage is opposite to the built-in electric field, the width of the depletion layer decreases, and carriers can easily transfer through the barriers, resulting in a high current. When the reverse voltage is applied to the device, the direction of the external voltage is the same as the built-in electric field, the width of the depletion layer increases, and the carrier transport is suppressed, resulting in a limited current [34]. The experimental results show that the device has a superior rectification characteristic, which is consistent with the analysis of the energy band diagram.

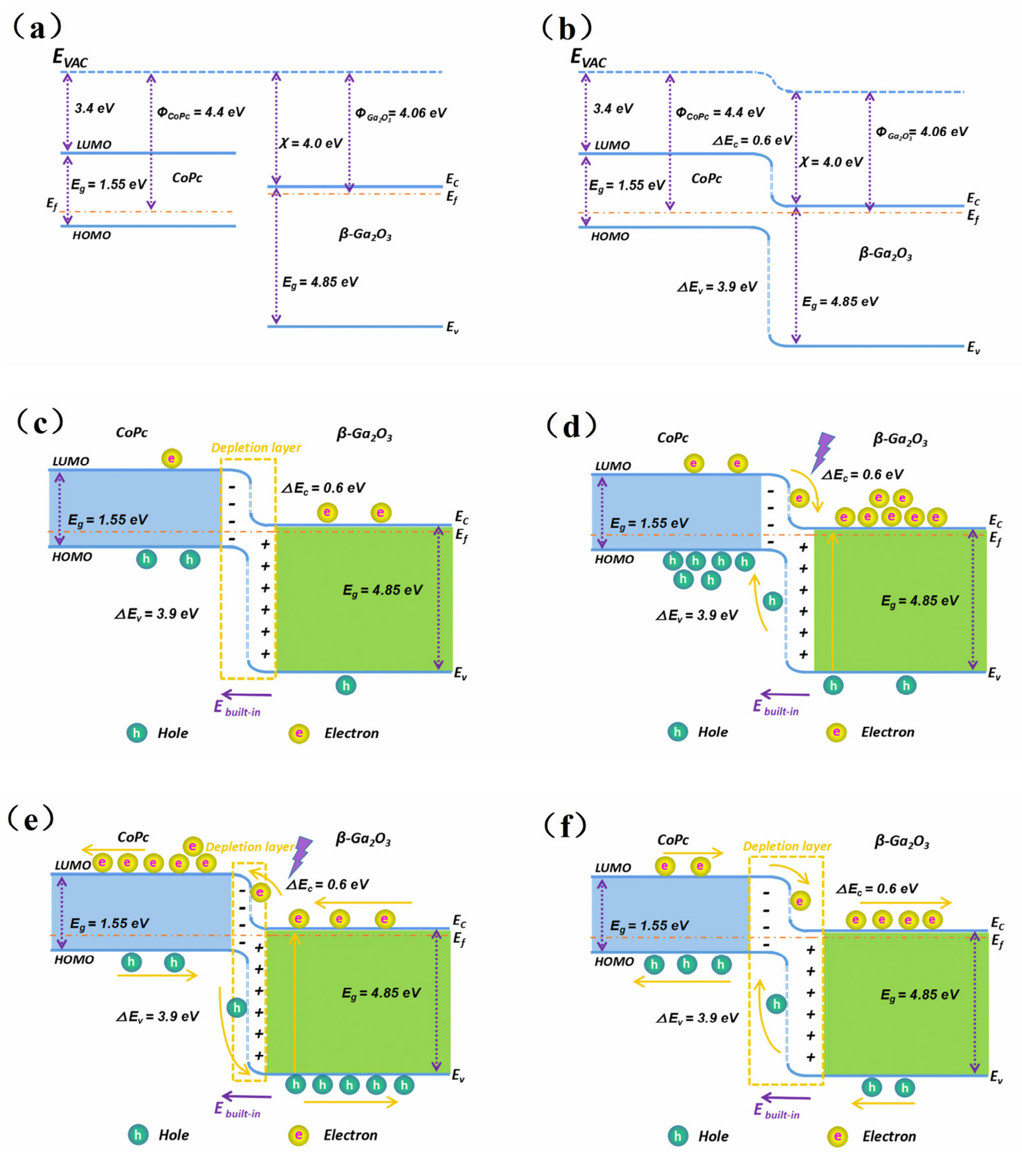

Figure 6. Schematic energy band diagrams of the CoPc/Ga_2O_3 heterostructure (**a**) before contact, (**b**) after contact, (**c**) under dark conditions, (**d**) with 254 nm light under 0 V, (**e**) with 254 nm light under forward voltages, and (**f**) with 254 nm light under reverse voltages.

4. Conclusions

In summary, an organic–inorganic hybrid heterojunction based on Ga_2O_3 and CoPc films was constructed into a planar ultraviolet photodetector. The device shows good wavelength selectivity and sensitivity to ultraviolet light, and it can work stably under different light intensities. The device has a dark current as low as 5.7 fA, which indicates its good immunity to interference. The device has a high D^* of 1.92×10^{17} Jones, an R of 18.4 mA/W, and a $PDCR$ of 3.76×10^6. Therefore, the prepared CoPc/Ga_2O_3 type-II heterojunction device may find great potential in ultraviolet detection, especially in weak light signals and noisy environments.

Author Contributions: X.Q. designed the experiments; X.Q. and S.Q. performed the experiments; X.Q., X.J. and J.Y. analyzed the data; J.W. contributed analysis tools; X.Q. wrote the paper, P.L. and W.T. supervised the process of the work. All authors have read and agreed to the published version of the manuscript.

Funding: This research was funded by the National Natural Science Foundation of China (Grant No. 61774019).

Data Availability Statement: Not applicable.

Conflicts of Interest: The authors declare no conflict of interest.

References

1. Tsao, J.Y.; Chowdhury, S.; Hollis, M.A.; Jena, D.; Johnson, N.M.; Jones, K.A.; Kaplar, R.J.; Rajan, S.; Van de Walle, C.G.; Bellotti, E.; et al. Ultrawide-Bandgap Semiconductors: Research Opportunities and Challenges. *Adv. Electron. Mater.* **2017**, *4*, 1600501. [CrossRef]
2. Zheng, W.; Huang, F.; Zheng, R.; Wu, H. Low-Dimensional Structure Vacuum-Ultraviolet-Sensitive (λ <200 nm) Photodetector with Fast-Response Speed Based on High-Quality AlN Micro/Nanowire. *Adv. Mater.* **2015**, *27*, 3921–3927. [CrossRef] [PubMed]
3. Zhang, Q.; Li, X.; He, Z.; Xu, M.; Jin, C.; Zhou, X. 2D semiconductors towards high-performance ultraviolet photodetection. *J. Phys. D Appl. Phys.* **2019**, *52*, 303002. [CrossRef]
4. Xie, C.; Lu, X.-T.; Tong, X.-W.; Zhang, Z.-X.; Liang, F.-X.; Liang, L.; Luo, L.-B.; Wu, Y.-C. Recent Progress in Solar-Blind Deep-Ultraviolet Photodetectors Based on Inorganic Ultrawide Bandgap Semiconductors. *Adv. Funct. Mater.* **2019**, *29*, 1806006. [CrossRef]
5. Zhou, C.; Ai, Q.; Chen, X.; Gao, X.; Liu, K.; Shen, D. Ultraviolet photodetectors based on wide bandgap oxide semiconductor films. *Chin. Phys. B* **2019**, *28*, 048503. [CrossRef]
6. Chen, X.; Ren, F.-F.; Ye, J.; Gu, S. Gallium oxide-based solar-blind ultraviolet photodetectors. *Semicond. Sci. Technol.* **2020**, *35*, 023001. [CrossRef]
7. Liu, Z.; Yu, J.; Li, P.; Wang, X.; Zhi, Y.; Chu, X.; Wang, X.; Li, H.; Wu, Z.; Tang, W. Band alignments of β-Ga_2O_3 with MgO, Al_2O_3 and $MgAl_2O_4$ measured by x-ray photoelectron spectroscopy. *J. Phys. D Appl. Phys.* **2019**, *52*, 295104. [CrossRef]
8. Xu, J.; Zheng, W.; Huang, F. Gallium oxide solar-blind ultraviolet photodetectors: A review. *J. Mater. Chem. C* **2019**, *7*, 8753–8770. [CrossRef]
9. Kaur, D.; Kumar, M. A Strategic Review on Gallium Oxide Based Deep-Ultraviolet Photodetectors: Recent Progress and Future Prospects. *Adv. Opt. Mater.* **2021**, *9*, 2002160. [CrossRef]
10. Baldini, M.; Galazka, Z.; Wagner, G. Recent progress in the growth of β-Ga2O3 for power electronics applications. *Mater. Sci. Semicond. Process.* **2018**, *78*, 132–146. [CrossRef]
11. Chen, M.; Zhao, B.; Hu, G.; Fang, X.; Wang, H.; Wang, L.; Luo, J.; Han, X.; Wang, X.; Pan, C.; et al. Piezo-Phototronic Effect Modulated Deep UV Photodetector Based on ZnO-Ga_2O_3 Heterojuction Microwire. *Adv. Funct. Mater.* **2018**, *28*, 1706379. [CrossRef]
12. Bae, H.; Charnas, A.; Sun, X.; Noh, J.; Si, M.; Chung, W.; Qiu, G.; Lyu, X.; Alghamdi, S.; Wang, H.; et al. Solar-Blind UV Photodetector Based on Atomic Layer-Deposited Cu_2O and Nanomembrane beta-Ga_2O_3 pn Oxide Heterojunction. *ACS Omega* **2019**, *4*, 20756–20761. [CrossRef] [PubMed]
13. Ding, W.; Meng, X. High performance solar-blind UV detector based on β-Ga_2O_3/GaN nanowires heterojunction. *J. Alloys Compd.* **2021**, *866*, 157564. [CrossRef]
14. Li, S.; Yan, Z.; Liu, Z.; Chen, J.; Zhi, Y.; Guo, D.; Li, P.; Wu, Z.; Tang, W. A self-powered solar-blind photodetector with largeVocenhancing performance based on the PEDOT:PSS/Ga2O3organic–inorganic hybrid heterojunction. *J. Mater. Chem. C* **2020**, *8*, 1292–1300. [CrossRef]
15. Kumar, A.; Prasad, R.; Debnath, A.K.; Singh, A.; Samanta, S.; Aswal, D.K.; Gupta, S.K. Growth and Electrical Transport Properties of Organic Semiconductor Thin Films. *Solid State Phenom.* **2013**, *209*, 1–5. [CrossRef]
16. Ma, Z.; Zhao, J.; Wang, X.; Yu, J. Effect of bulk and planar heterojunctions based charge generation layers on the performance of tandem organic light-emitting diodes. *Org. Electron.* **2016**, *30*, 136–142. [CrossRef]
17. Wahab, F.; Sayyad, M.H.; Nawaz Khan, D.; Tahir, M.; Aziz, F.; Shahid, M.; Ali Munawar, M.; Anwar Chaudry, J. Electrical characterization of cobalt phthalocyanine/p-silicon heterojunction. *Mater. Sci. Semicond. Process.* **2014**, *26*, 101–106. [CrossRef]
18. Bilgiçli, A.T.; Yaraşır, M.N.; Kandaz, M.; İlik, C.; Demir, A.; Bağcı, S. Nonperipheral tetra phthalocyanines bearing alkyl chain moiety; Synthesis, characterization and fabrication of the OFET based on phthalocyanine. *Synth. Met.* **2015**, *206*, 33–41. [CrossRef]
19. Jetly, A.; Mehra, R. Efficient Tandem Organic Light Emitting Diode Using Organic Photovoltaic Charge Generation Layer. *Int. J. Opt.* **2018**, *2018*, 9458530. [CrossRef]
20. Wahab, F.; Sayyad, M.H.; Khan, D.N.; Tahir, M.; Aziz, F.; Khan, R.; Karimov, K.S. Sensing Properties of Cobalt-Phthalocyanine-Based Multipurpose Sensor. *J. Electron. Mater.* **2016**, *46*, 2045–2052. [CrossRef]
21. Xiao, Y.; Liu, L.; Ma, Z.H.; Meng, B.; Qin, S.J.; Pan, G.B. High-Performance Self-Powered Ultraviolet Photodetector Based on Nano-Porous GaN and CoPc p-n Vertical Heterojunction. *Nanomaterials* **2019**, *9*, 1198. [CrossRef] [PubMed]
22. Liu, Z.; Li, S.; Yan, Z.; Liu, Y.; Zhi, Y.; Wang, X.; Wu, Z.; Li, P.; Tang, W. Construction of a β-Ga_2O_3-based metal–oxide–semiconductor-structured photodiode for high-performance dual-mode solar-blind detector applications. *J. Mater. Chem. C* **2020**, *8*, 5071–5081. [CrossRef]
23. Seoudi, R.; El-Bahy, G.S.; El Sayed, Z.A. Ultraviolet and visible spectroscopic studies of phthalocyanine and its complexes thin films. *Opt. Mater.* **2006**, *29*, 304–312. [CrossRef]

24. Liu, G.; Wang, Y.; Zhou, Y.; Cao, J.; Yuan, M.; Lv, H. Phosphorous doped g-C3N4 supported cobalt phthalocyanine: An efficient photocatalyst for reduction of CO_2 under visible-light irradiation. *J. Colloid Interface Sci.* **2021**, *594*, 658–668. [CrossRef] [PubMed]
25. Ma, G.-L.; Gao, A.; Liu, Z.; Sun, W.-M.; Li, S.; Yan, Z.-Y.; Jiang, W.-Y.; Sun, B.-Y.; Qi, X.-H.; Li, P.-G.; et al. Solution Spin-Coated $BiFeO_3$ Onto Ga_2O_3 Towards Self-Powered Deep UV Photo Detector of $Ga_2O_3/BiFeO_3$ Heterojunction. *IEEE Sens. J.* **2021**, *21*, 23987–23994. [CrossRef]
26. Dai, J.; Li, S.; Liu, Z.; Yan, Z.; Zhi, Y.; Wu, Z.; Li, P.; Tang, W. Fabrication of a poly(N-vinyl carbazole)/ϵ-Ga_2O_3 organic–inorganic heterojunction diode for solar-blind sensing applications. *J. Phys. D Appl. Phys.* **2021**, *54*, 215104. [CrossRef]
27. Li, S.; Guo, D.; Li, P.; Wang, X.; Wang, Y.; Yan, Z.; Liu, Z.; Zhi, Y.; Huang, Y.; Wu, Z.; et al. Ultrasensitive, Superhigh Signal-to-Noise Ratio, Self-Powered Solar-Blind Photodetector Based on n-Ga_2O_3/p-CuSCN Core-Shell Microwire Heterojunction. *ACS Appl. Mater. Interfaces* **2019**, *11*, 35105–35114. [CrossRef]
28. Yan, Z.; Li, S.; Liu, Z.; Zhi, Y.; Dai, J.; Sun, X.; Sun, S.; Guo, D.; Wang, X.; Li, P.; et al. High sensitivity and fast response self-powered solar-blind ultraviolet photodetector with a β-Ga_2O_3/spiro-MeOTAD p–n heterojunction. *J. Mater. Chem. C* **2020**, *8*, 4502–4509. [CrossRef]
29. Gao, A.; Jiang, W.; Ma, G.; Liu, Z.; Li, S.; Yan, Z.; Sun, W.; Zhang, S.; Tang, W. A self-powered β-$Ga_2O_3/CsCu_2I_3$ heterojunction photodiode responding to deep ultraviolet irradiation. *Curr. Appl. Phys.* **2022**, *33*, 20–26. [CrossRef]
30. Kokubun, Y.; Kubo, S.; Nakagomi, S. All-oxide p–n heterojunction diodes comprising p-type NiO and n-type β-Ga_2O_3. *Appl. Phys. Express* **2016**, *9*, 091101. [CrossRef]
31. Fatima, N.; Ahmed, M.M.; Karimov, K.S.; Ahmad, Z.; Muhammad, F.F. Optical sensors based on the NiPc–CoPc composite films deposited by drop casting and under the action of centrifugal force. *Chin. Phys. B* **2017**, *26*, 060704. [CrossRef]
32. Klein, A. Energy band alignment at interfaces of semiconducting oxides: A review of experimental determination using photoelectron spectroscopy and comparison with theoretical predictions by the electron affinity rule, charge neutrality levels, and the common anion rule. *Thin Solid Films* **2012**, *520*, 3721–3728. [CrossRef]
33. Wang, Y.; Tang, Y.; Li, H.; Yang, Z.; Zhang, Q.; He, Z.; Huang, X.; Wei, X.; Tang, W.; Huang, W.; et al. p-GaSe/n-Ga_2O_3 van der Waals Heterostructure Photodetector at Solar-Blind Wavelengths with Ultrahigh Responsivity and Detectivity. *ACS Photonics* **2021**, *8*, 2256–2264. [CrossRef]
34. Li, P.; Shi, H.; Chen, K.; Guo, D.; Cui, W.; Zhi, Y.; Wang, S.; Wu, Z.; Chen, Z.; Tang, W. Construction of GaN/Ga_2O_3 p–n junction for an extremely high responsivity self-powered UV photodetector. *J. Mater. Chem. C* **2017**, *5*, 10562–10570. [CrossRef]